New Regimes of Magnetic Reconnection in Collisionless Plasmas

Dennis W. Hewett, Gregory E. Frances, and Claire E. Max
Physics Department and Institute of Geophysics and Planetary Physics, Lawrence Livermore National Laboratory, University of California, Livermore, California 94550
(Received 18 December 1987)

An implicit particle-in-cell code has been used to study collisionless magnetic reconnection of a current sheet. The reconnection process is found to occur in three distinct stages: (1) early spontaneous reconnection fed by the free energy of an initial anisotropy in the electron component; (2) coalescence of the resulting small-scale filaments of electron current, accompanied by electron jetting; and (3) oscillatory flow of electrons through the magnetic X point, superposed on continuing nonlinear growth of ion-mediated reconneciton. The time evolution of stage 3 is strongly dependent on M_i/m_e.

PACS numbers: 94.30.Ej, 52.65.+z, 94.30.Ch, 94.30.Fk

We study the evolution of magnetic field reconnection in a collisionless plasma neutral sheet, using implicit particle-in-cell (PIC) computer simulations. The general two-dimensional collisionless neutral sheet configuration is thought to be of relevance to the magnetotails of the Earth and other magnetized planets, where reconnection is associated with magnetic substorms[1]; and to the eventual fate of tangled magnetic field lines in collisionless astrophysical plasmas, in which estimates of the thermal conductivity depend sensitively on the largely unknown rate of field-line reconnection.[2] The specific parameters of our simulation are quite close to plasma conditions in the laboratory reconnection experiments of Stenzel and Gekelman.[3]

In simplest form, reconnection in a *collisional* plasma can be modeled with the MHD equations with a fixed value for the plasma resistivity. This yields a reduced, one-fluid description in which the large-scale topology and dynamics of reconnecting regions can be studied. By contrast, *collisionless* reconnection of magnetic field lines depends on electron inertia effects and the detailed behavior of the electron distribution function to provide the necessary freedom for magnetic topology changes. The formation of a non-Maxwellian tail on the ion distribution can be an important observed consequence of collisionless reconnection. Hence a faithful computational model must include a kinetic description of both electrons and ions.

Although traditional explicit PIC techniques provide this description, stability requirements restrict simulation parameters to artificially small ion-to-electron mass ratios (e.g., $M_i/m_e \approx 10$ to 25), and short temporal periods (e.g., 100 plasma periods ω_{pe}^{-1} or less).[4] In the present Letter a new 2.5D fully electromagnetic direct implicit PIC plasma simulation code AVANTI[5] allows us to follow the dynamics of collisionless reconnection for all relevant M_i/m_e, and for a factor of 2 to 3 longer time scales. Details of this method can be found in Hewett and Langdon[5] and references therein. Since we are no longer constrained to resolve purely electromagnetic modes or ω_{pe} oscillations, we typically use $\omega_{pe}\Delta t \approx 1$-2. Overall, we estimate that this implicit technique has expanded the parameter regime that can be studied by at least an order of magnitude. We have exploited this new advantage to simulate physically realistic mass ratios that reveal qualitatively new behavior.

The simulation region consists of 40 times 96 x-y mesh, with all quantities initially uniform in y. Starting with a constant ion temperature and a Gaussian ion density profile, we derive the initial equilibrium fields shown in Fig. 1(a). The initial neutral sheet width δ is $2c/\omega_{pe}$. Larmor radii for electrons and ions outside of the neutral sheet are $\rho_e = 0.4c/\omega_{pe}$, and $\rho_i = 20c/\omega_{pe}$, respectively. By way of comparison, the laboratory reconnection experiments of Stenzel and Gekelman[6] typically use $\delta = 3c/\omega_{pe}$, $\rho_e = 0.4c/\omega_{pe}$ and $\rho_i = 2c/\omega_{pe}$. The x gradient in magnetic pressure near the neutral sheet is balanced by gradients in electron and ion particle density. Periodic boundary conditions are imposed at the top and bottom of the box. At the sides of the box, fields and particle densities approach values that are constant with x. Boundary conditions at the sides are perfect reflection for particles, Dirichlet conditions for **E**, and Neumann conditions for **B**.

This equilibrium resembles the Harris equilibrium,[7] but the ions carry no current, and are electrostatically confined. We also allow for anisotropy in electron temperatures parallel ($T_{e\parallel}$) and perpendicular ($T_{e\perp}$) to the initial magnetic field. Following the work of Chen and Palmadesso,[8] we allow a cooler $T_{e\parallel}$ to trigger the initial stages of reconnection.

Figure 1(b)-1(d) shows the time evolution of the magnetic field topology for a typical simulation. Contours of magnetic flux are shown as solid lines; the innermost (dotted) contour is the "separatrix," inside of which lies magnetic flux that has become trapped due to reconnection. Frame 1(b) shows the magnetic configuration characteristic of the early stages of reconnection, before the ions have had time to move. The electron current at the neutral sheet has already formed

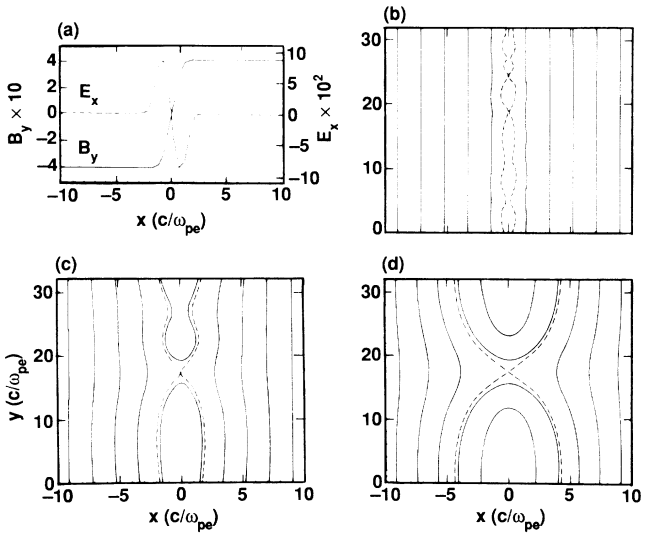

FIG. 1. (a) Profiles of initial electrostatic field E_x (dashed) and magnetic field B_y (solid) across the neutral sheet. Both fields have units of $m_e c\omega_{pe0}/e$. The sheet current in the z direction is carried by electrons. Ions are contained by the electrostatic field. The initially uniform electron and ion temperatures are $T_{e\perp}/m_e c^2 = 2.8\times10^{-2}$, $T_{e\parallel} = \frac{4}{9} T_{e\perp}$, $T_i/m_e c^2 = 8.0 \times 10^{-2}$.(b)–(d). Magnetic flux contours (solid) and separatrix (dotted) in x-y plane: $t = 30\omega_{pe}^{-1}$, showing small-scale electron-driven filaments; (c) $t = 160\omega_{pe}^{-1}$, as coalescence begins; (d) $t = 410\omega_{pe}^{-1}$, with only one X point remaining.

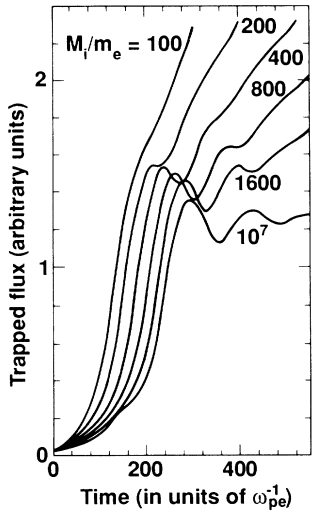

FIG. 2. Trapped magnetic flux vs time, for six different M_i/m_e. In all cases, $T_{e\parallel}/T_{e\perp} = \frac{4}{9}$ initially. The long-time linear growth is proportional to $M_i^{-1/2}$.

small-scale filaments, resulting in several magnetic X points within the simulation volume. Later, Fig. 1(c) shows that some of these small-scale filaments have coalesced. Still later, when enough time has passed for ion dynamics to become important, we see one remaining magnetic island, as in Fig. 1(d). This stage of the process is typically reached in approximately 1–3 Alfvén transit times. The remaining O point continues to grow in amplitude, for our parameters, until the separatrix approaches the boundaries of the simulation box. The simulation is then terminated; further results would be artifacts of the boundary conditions.

A normal component of the electric field (E_z) develops as the small-scale current filaments coalesce; this field is responsible for the $\mathbf{E}\times\mathbf{B}$ drift of the electrons (but not the unmagnetized ions) into the final O point through the X point. The resulting electron current in the x-y simulation plane generates a normal component of the magnetic field (B_z) with quadrupole structure. Hoshino[9] showed that the suppression of this quadrupole field does not affect the rate of magnetic reconnection, suggesting that B_z is not a cause, but an effect, of the reconnection process.

Simulations with large ion-to-electron mass ratio ($M_i/m_e \geq 200$) reveal an oscillation in sign of the normal B_z quadrupole. The cause is an oscillation in the electron flow through the X point. Since the magnetic field is "frozen" into the electron component, the magnitude of trapped magnetic flux will also oscillate as the electrons flow into and out of the O point. Observation of trapped flux as a function of time for various M_i/m_e provides information about the moderating influence of the ions on the electron oscillation. These curves are shown in Fig. 2 for six different values of M_i/m_e.

Late in time after the oscillations damp out, the trapped flux grows approximately linearly in time, at a rate proportional to the ion-acoustic speed, $v_s = (kT_e/M_i)^{1/2}$. (Consistent with this scaling, in the limit $M_i/m_e \rightarrow \infty$ the trapped flux experiences simple oscillation with no secular growth.) This late-time oscillation and secular growth of trapped flux is a qualitatively different phenomenon than has been reported in previous studies.[4] Previous investigators, using $M_i/m_e = 10$–25, saw the coalescence of small-scale magnetic islands and sometimes saw oscillatory behavior when the island began to interact with the outer wall. Inadequate separation between the ion and electron time scales would obscure the late-time oscillations that we see resulting from charge-separation electric fields and from $\mathbf{E}\times\mathbf{B}$ forces, superposed on continued secular growth of trapped flux (Fig. 2).

The nature of the three temporal regions described above for $M_i/m_e > 200$ can be clarified by an idealized simulation having $T_{e\parallel}/T_{e\perp} = 0$, and $M_i/m_e = 2000$. Figure 3 shows the time evolution of (a) trapped magnetic flux, (b) quadrupole z component of magnetic field, (c) electron flow energy in the y and z directions, and (d) z components of electric field and current. Region I, in which the trapped flux grows linearly with time, corresponds to the early electron-driven formation of small-scale current filaments as evidenced in Fig. 1(b). Region II corresponds to the coalescence of the small-scale mul-

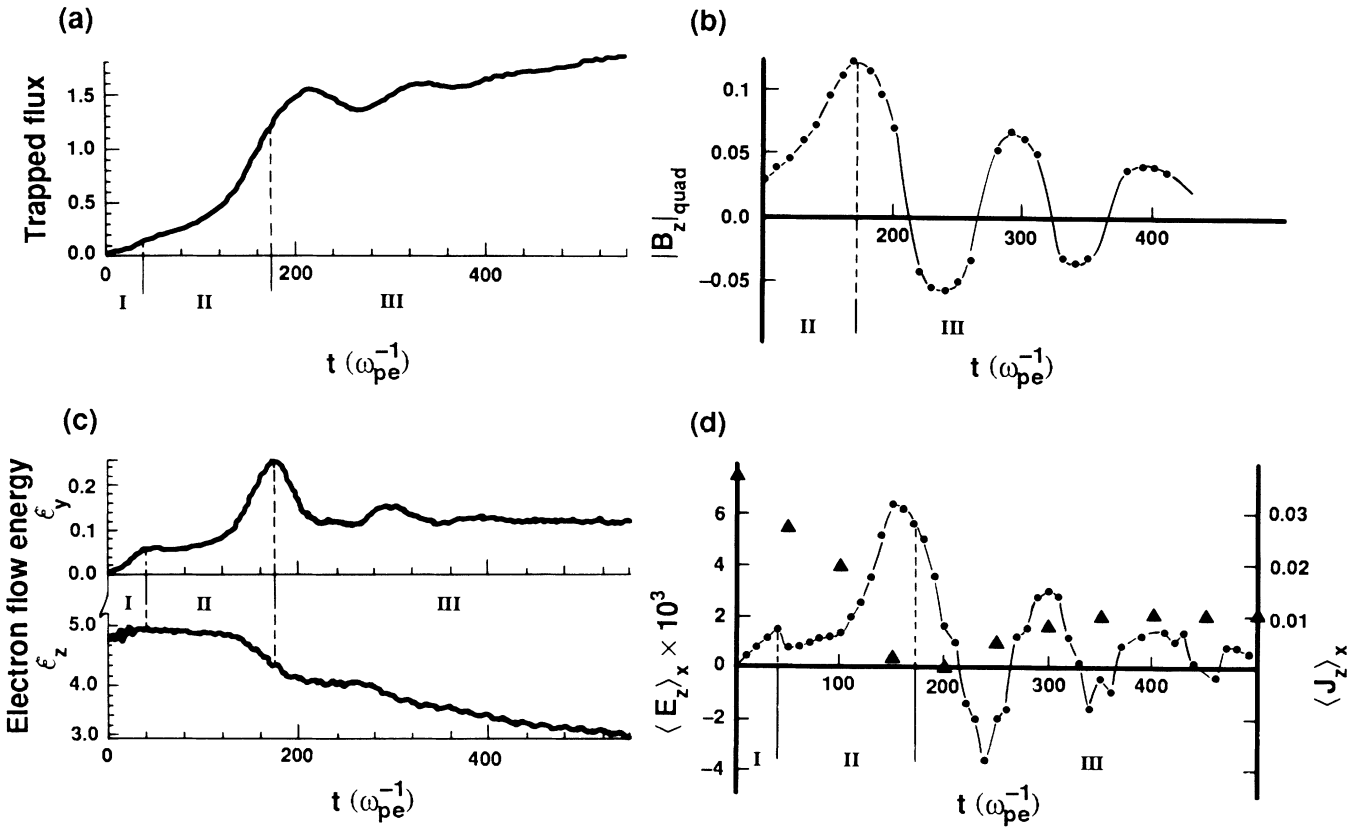

FIG. 3. Time evolution of an idealized simulation with initial $T_{e\parallel}/T_{e\perp}=0$ and $M_i/m_e=2000$: (a) trapped magnetic flux; (b) peak-to-peak amplitude of quadrupole magnetic field B_z; (c) electron flow energy in the y and z directions vs time; (d) E_z (dots) and J_z (triangles) at the y position of the X point, averaged over x.

tiple X points, and shows exponential growth of trapped flux. The end of region II is signaled by a peak in y-directed electron energy consistent with jetting, and a corresponding reduction of the z-directed energy caused by the E_z required for the jetting. In Region III, ions play the decisive role: An ambipolar electric field between the electrons and much-more-massive ions reverses the electron flow, causing oscillations back and forth from the external region through the X point to the O point. These oscillations are seen most clearly in Fig. 3(b).

The oscillations that are evident in the z component of the electric field, Fig. 3(d), are not found in the z component of the current. In fact, there is no proportionality at all between the time behaviors of E_z and J_z. The z components of the current and electric field do not even occupy the same volume in our simulations. Early in the reconnection process the electrons that carry J_z move away from the X points, and subsequent currents flow in the vicinity of the O points. This behavior is seen in laboratory reconnection experiments as well.[10] Even if there were an "anomalous resistivity" η, the rate of dissipation ηJ^2 would be quite small at the X point, since J_z is small there. Thus the MHD picture with an anomalous resistivity η acting on the z component of current at the X point seems to be qualitatively incorrect for the cases we have examined here. There remains, however, the more speculative possibility that "anomalous" dissipation might operate on the oscillating electron currents in the x-y plane.

The results of the present work agree qualitatively with behavior seen in previous computer simulations[4] at early and intermediate times: (1) initial formation of small-scale magnetic islands, and (2) rapid coalescence of these into larger structures, with concomitant development of a driving E_z. We observe a new type of behavior at later times, for ion-to-electron mass ratios above 200: oscillatory electron currents through the X point in the x-y plane, superimposed on linear (not exponential) growth of trapped flux at a rate proportional to $(T_e/M_i)^{1/2}$.

The linear, rather than exponential, growth of trapped flux evident at very early times [Region I of Fig. 3(a)] may be due in part to the extreme initial anisotropy ($T_{e\parallel}/T_{e\perp}=0$). We believe, however, that it is more closely associated with the high noise level in the particle initialization, resulting from the limited number of simulation particles ($N_e=N_i=27000$). Further study of

this stage with more reasonable anisotropy ($T_{e\parallel}/T_{e\perp} = \frac{4}{9}$) and an order of magnitude more particles ($N_e = N_i = 232000$) shows exponential growth consistent with the linear collisionless electron-driven tearing mode instability.[11] These results will be reported elsewhere.

Our simulations indicate that the region showing oscillatory behavior [Region III of Fig. 3(a)] is one in which an electron current flows into and out of the O points through the X points. The ions attempt to follow the electron current, pulled by an ambipolar electric field. But only for small ion-to-electron mass ratios (< 200) can they succeed in doing so before the electron flow reverses. Such behavior emphasizes that in our simulations the magnetic flux is frozen into the *electron* component rather than the plasma as in the usual MHD formulation.

Finally, near the end of our simulation the growth of trapped flux occurs with one dominant mode in B_x, because shorter-wavelength modes have already undergone coalescence. Thus theories of nonlinear saturation which rely on the presence of many modes of k space[12,13] are not applicable here. The late-time amplitudes are large in our simulations: $\langle B_x\rangle/B_0 \sim (\sqrt{2}\rho_e/\delta)^{-1} \sim 0.3$ at time $600\omega_{pe}^{-1}$. In addition, $\langle B_x\rangle$ continues to increase at late times in the simulation, with trapped flux growing linearly with time. This late-time continued growth, which has not been reported in previous PIC computer simulations, qualitatively resembles the Sweet-Parker phase predicted for MHD reconnection,[14] and would be a particularly interesting case for further analysis.

This research was performed under the auspices of the U.S. Department of Energy by the Lawrence Livermore National Laboratory under Contract No. W-7405-ENG-48.

[1]F. V. Coroniti and C. F. Kennel, J. Geophys. Res. **77**, 3361 (1972), and in *Cosmic Plasma Physics,* edited by K. Schindler (Plenum, New York, 1972), p. 15; C. T. Russell and R. L. McPherron, Space Sci. Rev. **15**, 205 (1973); K. Schindler, in *Dynamics of the Magnetosphere,* edited by S.-I. Akasofu (Reidel, Hingham, MA, 1980), p. 311.

[2]L. L. Cowie and C. F. McKee, Astrophys. J. **211**, 135 (1977).

[3]R. L. Stenzel and W. Gekelman, J. Geophys. Res. **86**, 649 (1981); W. Gekelman and R. L. Stenzel, J. Geophys. Res. **86**, 659 (1981).

[4]J. N. Leboeuf, T. Tajima, and J. M. Dawson, Phys. Fluids **25**, 784 (1982); J. N. Leboeuf *et al.*, in *Magnetic Reconnection in Space and Laboratory Plasmas,* edited by E. W. Hones (American Geophysical Union, Washington, DC, 1984), p. 282; M. Hoshino, J. Geophys. Res. **92**, 7368 (1987).

[5]D. W. Hewett and A. B. Langdon, J. Comput. Phys. **72**, 121 (1987).

[6]R. L. Stenzel and W. Gekelman, Phys. Rev. Lett. **42**, 1055 (1979).

[7]E. G. Harris, Nuovo Cimento **23**, 115 (1962).

[8]J. Chen and P. Palmadesso, Phys. Fluids **27**, 1198 (1984).

[9]Hoshino, Ref. 4.

[10]W. Gekelman and H. Pfister, Bull. Am. Phys. Soc. **32**, 1753 (1987).

[11]G. Laval, R. Pellat, and M. Vuillemin, in *Plasma Physics and Controlled Nuclear Fusion Research* (IAEA, Vienna, 1966), Vol. 2, p. 259; see also summary in Hones (Ref. 4), pp. 311–315.

[12]F.V. Coroniti, Phys. Rev. Lett. **38**, 1355 (1977).

[13]D. Biskamp, R. Z. Sagdeev, and K. Schindler, Cosmic Electrodynamics **1**, 297 (1970).

[14]E. N. Parker, *Cosmical Magnetic Fields* (Clarendon, Oxford, 1979), Chap. 15.